

ON THE UNDERSTANDING OF THE Q-SLOPE OF NIOBIUM THIN FILMS

S. Aull*, CERN, Geneva, Switzerland and Universität Siegen, Germany
 T. Junginger, A. Sublet, W. Venturini Delsolaro, P. Zhang, CERN, Geneva, Switzerland
 A.-M. Valente-Feliciano, Jefferson Lab, Newport News, VA, USA
 J. Knobloch, Helmholtz-Zentrum Berlin and Universität Siegen, Germany

Abstract

The Q-slope of niobium coated copper cavities at medium fields is still the limiting factor for the application the Nb/Cu technology in accelerators. This paper presents a dedicated study of a niobium coating with bulk-like characteristics which shows a Q-slope comparable to bulk Nb at 400 MHz and 4 K. Combining the bulk like film with recent findings of the HIE Isolde indicates that the film microstructure and the Nb/Cu interface are the key aspects to understanding the Q-slope.

INTRODUCTION

The proposal of building superconducting RF cavities from copper and coat the inner surface with a 1 μm to 2 μm thin niobium film goes back to 1984 [1]. The niobium film technology benefits from several advantages over bulk niobium: The copper substrate provides excellent thermal stability which not only prevents the cavity from thermal runaway but also allows to increase the wall thickness to mitigate microphonics. Moreover, the film parameters can be tuned to optimize the BCS resistance which has a minimum for a residual resistance ration (RRR) between 10 and 30 and increases towards higher and lower RRR values [2]. In contrast to the low RRR Nb/Cu films, bulk Nb cavities require high (bulk) RRR as the thermal conductivity is proportional to it. Nb/Cu films are also known to have a low sensitivity to trapped flux. Hence, coated cavities allow reducing the complexity of cryomodules as they do not require magnetic shielding [3]. In addition to physical advantages, Nb/Cu technology allows reducing raw material costs.

Nevertheless, Nb/Cu cavities suffer from a strong, usually exponential, increase of the surface resistance with increasing RF field. This *Q-slope* currently limits the application of Nb/Cu technology to accelerating gradients as low as 10 MV/m. Although the Q-slope is present throughout all Nb/Cu projects, from big (352 MHz) four cell elliptical cavities like LEP2 through small single cell elliptical cavities like CERN's 1.3 GHz/1.5 GHz R&D programme to the quater-wave resonators at 101 MHz of the HIE-Isolde project, the cause is still not well understood and subject to recent research activities.

In the 1990's, CERN launched a vigorous R&D programme for coating single cell 1.5 GHz cavities with dc magnetron sputtering. The study focussed on the influence of coating parameters such as type and mixtures of the work-

ing gas(es) and the surface preparation on the BCS and residual surface resistance and the Q-slope [4]. The Nb/Cu research was put on hold in 2001 and relaunched in 2008 for the development of Nb coated quaterwave resonators for the HIE-Isolde project [5].

Until today, several laboratories around the world have (re-)joint the efforts on improving the Nb/Cu technology and on understanding and curing the Q-slope. Based on the work done in the 90's, the community pushes for denser films and improved Nb/Cu interfaces [6–10]

MICROSTRUCTURE OF THE HIE ISOLDE COATINGS

The Nb/Cu technology was chosen for the superconducting cavities for the High Intensity and Energy (HIE) upgrade of the Isolde facility at CERN [5].

The quater-wave resonators are made from bulk OFE copper and are coated using DC-bias diode sputtering. Details on the coating technique can be found elsewhere [11]. The HIE Isolde cavity $Q4$ is a mockup cavity of the same geometry as the RF cavities which allows coating small samples in various positions throughout the cavity surface [12]. The coatings on these samples represent the coating on the RF cavity and are used for dedicated studies on correlating the microstructure of the film with the RF performance.

A focussed ion beam (FIB) can be used to cut a crate into a coating and investigate the cross-section of the film with a scanning electron microscope (SEM) [13]. Figures 1(a) and 1(b) show two FIB-SEM images of a typical HIE Isolde coating according to the standard recipe with a bias of -80 V. Both images show the microstructure of the coating close to the top of the cavity. The geometry and the vicinity to the electron beam weld make this region the most delicate to coat: Figure 1(a) corresponds to the position $e9$ on the outer conductor, close to the electron beam weld and shows intergranular porosity and a rough surface. In contrast to that Figure 1(b) shows the film microstructure in position TBi , on the top band on top of the cavity. No porosity in the RF exposed layer is visible, but the film shows voids at the interface with the copper substrate.

In order to reduce the porosity, the bias was increased to -120 V. The RF performance of the cavity coated with this high bias was however poor. Figure 2 compares the surface resistance as function of RF field for a standard coating with the high bias coating. The measurements are done at 4.5 K at resonance frequency of 101 MHz. FIB-SEM images on the high bias coating revealed that the coating was indeed

* sarah.aull@cern.ch



Figure 1: FIB-SEM images of (a) a porous film; (b) a film with voids at the interface; (c) a partially delaminated film.

much less porous, but the film partially delaminated from the substrate as shown in Figure 1(c) for position *i4*, in the centre of the inner conductor. It is assumed that the high bias induced significantly more stress to the film which caused the delamination. Further details about the effect of the higher bias on the microstructure can be found in [11].

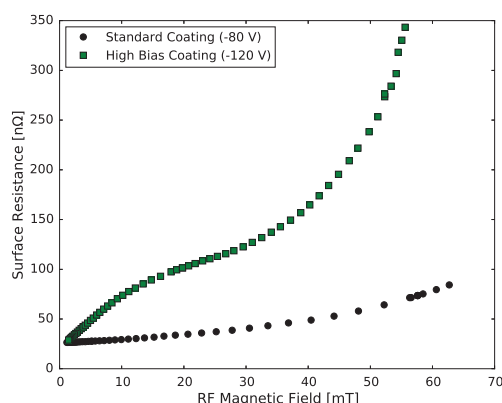


Figure 2: Surface Resistance at 4.5 K and 101 MHz of a typical HIE-Isolde coating compared to the coating with high bias.

ELECTRON CYCLOTRON RESONANCE

With conventional physical vapour deposition (PVD) techniques, control over the deposition process is exercised by only four first-order parameters: the absolute arrival rates of film atoms, the partial pressures of background gases in the chamber, the energy of the deposition fluxes and the substrate temperature. The ions produced by these techniques have typically an energy of less than 10 eV. Without energetic atoms, only the substrate temperature influences the different processes involved in film deposition, i.e. physio- and chemisorption, thermal desorption, nucleation, nuclei dissociation, surface diffusion, and formation of specific nucleation sites. Crystalline defects, grains connectivity and grain size may be improved with a higher substrate temperature which provides higher surface mobility. However practical substrates for SRF cavities (Al, Cu) may not allow heating to high temperatures. The missing energy may be supplied by ion bombardment. Energetic condensation is a deposition process where a significant fraction of the

condensing species have hyper-thermal and low energies (10 eV and greater). It is characterized by a number of surface and sub-surface processes that are activated or enabled by the energy of the ions arriving at the surface [14]. In order to explore the benefits of energetic condensation for SRF applications, JLab has developed an ECR ion source to generate niobium ions inside vacuum [15]. An electron beam gun is used to create a dense neutral niobium flux, and an ECR chamber is used to convert the neutral niobium vapor to a niobium plasma. The ECR chamber is made of a copper cylinder inserted into two slightly separated copper coils which are used to form a magnetic field with a specific strength (87.5 mT) and profile. The ECR chamber, copper coils and the electron gun sit in the vacuum chamber. An electric field via an RF generator (magnetron) is established perpendicular to the magnetic field created by the copper coils. The niobium plasma is created when the electrons in the ECR chamber resonate with the RF field and are accelerated to their cyclotron resonance. This leads to an almost complete ionization producing niobium ions with a nominal energy of 64 eV. These energetic niobium ions are extracted to a biased substrate. The deposition energy is then simply controlled by the substrate bias voltage. The ECR plasma deposition of Nb has the potential to produce superior quality Nb films as it brings undeniable advantages compared to other PVD techniques, such as:

- Production of high flux of singly charged Nb ions under vacuum
- Absence of carrier gas leading to freedom from gas inclusions
- Absence of macro-particle production
- Control of the ion energy with applied bias to the substrate
- Quasi-conformal deposition

These factors are very useful to accomplish careful investigations of the film growth dynamics [16]. Thus far, it has been shown that the microstructure of Nb films can be altered with incident ion energy and the RRR, a gauge of the mean free path, can be tuned from single digits to as high as 725. The optimum incident ion energy depends on the substrate

nature and the coating temperature. The ECR Nb films typically exhibit dense grain boundaries and good adhesion to the substrate.

ECR Nb/Cu FOR THE QUADRUPOLE RESONATOR

For an extensive study on the SRF performance, a sample was coated for testing in CERN's Quadrupole Resonator (QPR). The QPR is a four wire transmission line in which a flat sample with a diameter of 75 mm can be characterized. Using a calorimetric method, the surface resistance can be measured as function of temperature and RF field (up to 65 mT) at 400 MHz, 800 MHz and 1200 MHz. A detailed description can be found elsewhere [17–19].

Sample Preparation

The sample was prepared as follows: An OFHC copper substrate was machined and mechanically polished to a mirror finish surface. It was then electron beam welded (EBW) to a ring of bulk niobium which was welded to the support structure after coating. To remove embedded polishing material and to recover the crystal structure, the sample disk was electro-polished with a removal of 14 μm and then shipped to Jefferson Lab for coating.

The QPR sample was mounted along with witness samples (fine grain and large grains OFHC Cu and (11 $\bar{2}$ 0) Al_2O_3) on a resistively heated Cu sample holder, electrically isolated to allow biasing. The samples were baked and coated in-situ at 360 $^\circ\text{C}$. This baking temperature allows to dissolve the native CuO layer into the Cu bulk, providing an epitaxial surface for Nb deposition. The nucleation and early growth phases (first 100 nm) were performed at an ion energy of 184 eV and followed by a subsequent growth at 64 eV for the remainder of the film thickness. The Cu fine grain and sapphire witness samples exhibited a RRR of respectively 122 and 201, measured by the 4-point probe method.

After coating, the sample was EBW to the support structure. It should be noted that the weld is along the bottom edge of the Nb ring and not on the actual coating. A certain heating of the substrate and the Nb film could however not be avoided.

The whole sample ensemble was then rinsed in a clean room with ultra pure water at 6 bar, mounted in the QPR in front of a laminar flow box and then cooled down for RF testing.

Microstructure of the ECR Film

Along with the sample for the QPR, a set of witness samples on equivalent substrates were coated. The grain size and orientation of the coating was derived using electron backscatter diffraction (EBSD). The resulting crystal map is shown in Figure 3. The grain size is as typical for copper in the order of 50 μm . It is therefore concluded that the Nb copies the crystal structure from the substrate as expected.



Figure 3: EBSD map of the ECR Nb/Cu coating. The average grain size is about 50 μm .

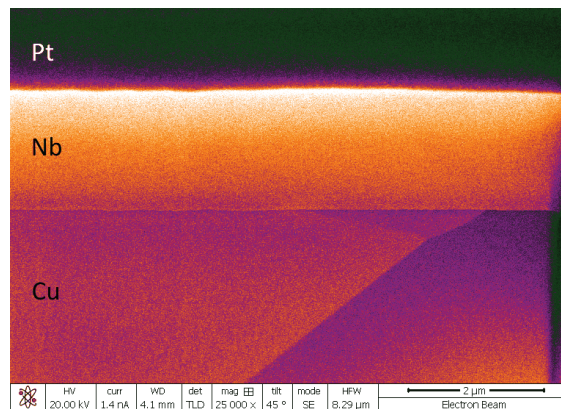


Figure 4: FIB-SEM across the ECR coating. The platinum film serves as a protection layer from the ion beam. Courtesy of R. Valizadeh.

Scanning electron microscopy (SEM) on the actual QPR sample confirmed a grain size of 50 μm [20].

FIB-SEM on the cross-section of the film revealed the micro-structure in the depth of the film and at the copper interface. Two FIB-SEM images are displayed in Figures 4 and 5. It can be seen that the coating has not only a very smooth surface but also a very smooth interface with the copper substrate. In contrast to the copper, no niobium grain boundary is visible over the entire FIB crate of about 15 μm . This indicates that the big grain size derived from the EBSD and surface SEM is not a surface feature but represents also the bulk grain structure. Moreover, no porosity or delamination or any kind of other substructure is visible down to a scale of single nanometer.

We conclude that in terms of crystal structure this ECR coating is bulk-like.

SRF PERFORMANCE OF THE ECR FILM

The SRF performance is quantified by measuring the surface resistance and other superconducting resp. material parameters. All QPR measurements were performed on the ECR coating and a reactor grade bulk niobium sample for comparison.

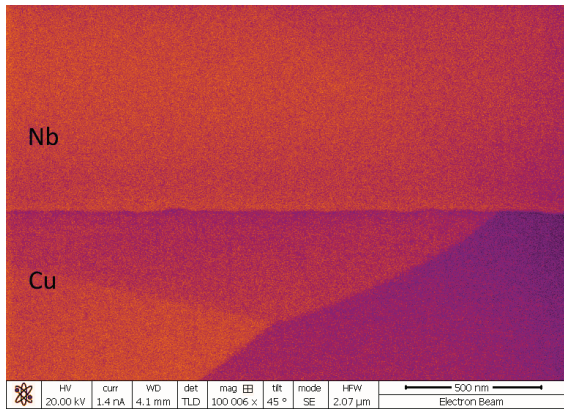


Figure 5: FIB-SEM across the ECR coating. Courtesy of R. Valizadeh.

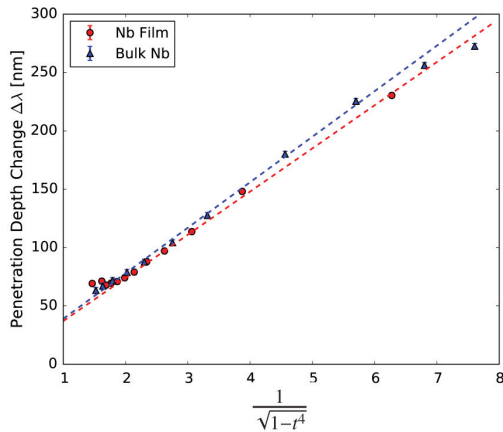


Figure 6: Penetration depth measurement of the ECR coating and a reactor grade bulk niobium sample.

Low Field Characteristics

From measuring the shift in resonance frequency with temperature the penetration depth change, $\Delta\lambda$, can be calculated and the penetration depth at 0 K, λ_0 , as well as the critical temperature, T_c , can be derived. Figure 6 shows the penetration depth change as a function of the Gorter-Casimir expression:

$$\lambda(T) = \frac{\lambda_0}{\sqrt{1-t^4}} \quad (1)$$

where $t = T/T_c$ and $\Delta\lambda = \lambda(T) - \lambda_0$.

Using Pippard's expression [21],

$$\lambda(0\text{ K}, \ell) = \lambda_L \sqrt{1 + \frac{\pi\xi_0^2}{2\ell}}, \quad (2)$$

the mean free path, ℓ , can be calculated from the penetration depth at 0 K. Here, λ_L is the London penetration depth and describes the penetration depth at 0 K and for infinite mean free path. ξ_0 is the BCS coherence length and has, like λ_L , to be taken from literature. According to [2], we choose $\lambda_L = 32$ nm and $\xi_0 = 39$ nm. The corresponding RRR is estimated via $\ell[\text{nm}] = 2.7 \cdot \text{RRR}$. The derived

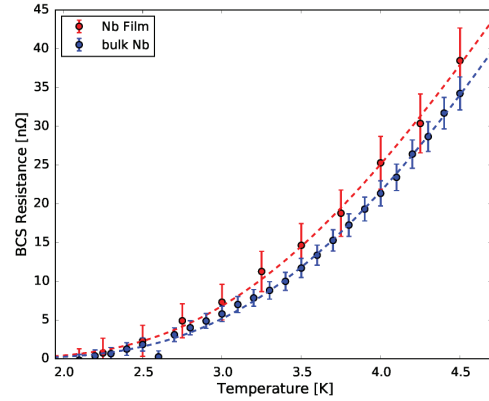


Figure 7: BCS Resistance of the ECR coating and a reactor grade bulk niobium sample.

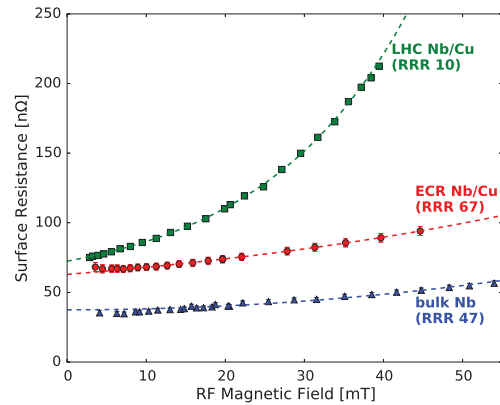


Figure 8: Surface resistance as function of RF magnetic field at 4 K and 400 MHz. The ECR coating is compared to a typical LHC coating and bulk Nb. Dashed lines indicate exponential (LHC & ECR) and quadratic (bulk Nb) fits.

material parameters are listed in Table 1 and we find that all parameters are similar for both samples.

For both samples the surface resistance was measured as a function of temperature at 400 MHz. The RF field was kept constant at about 10 mT so that the field dependence can be neglected. From an exponential fit, the low field residual resistance at 0 K as well as the superconducting energy gap can be extracted. The resulting values are listed in Table 1.

Figure 7 shows the BCS resistance, i.e. the measured surface resistance with subtracted residual resistance from the fit, for both samples. As can be seen, the increase in surface resistance with temperature is very similar but slightly higher for the ECR coating. This is consistent with slightly longer mean free path and larger energy gap of the niobium film.

Also in terms of low field superconducting (RF) properties, we consider the ECR coating as bulk-like.

Table 1: Superconducting properties of the ECR coating compared to a reactor grade bulk Nb sample. All values have been measured with the QPR or are derived from these measurements.

	ECR Nb/Cu	bulk Nb
Penetration Depth λ_0 [nm]	37 ± 2	39 ± 2
Mean free path [nm]	182 ± 24	126 ± 18
RRR	67 ± 9	47 ± 7
Critical temperature [K] from $f(T)$ measurement	9.36 ± 0.01	8.99 ± 0.01
Residual resistance at 400 MHz [n Ω]	30.03 ± 0.07	19.1 ± 0.1
Energy gap $\Delta/k_B T_c$	1.97 ± 0.06	2.07 ± 0.02

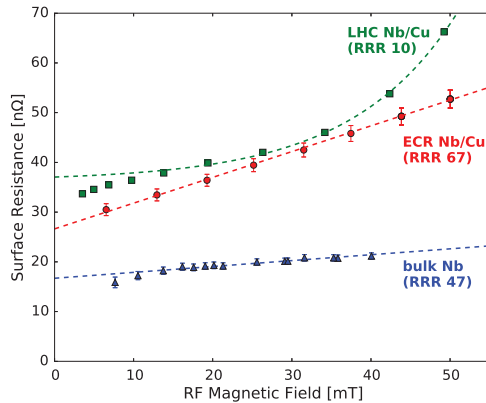


Figure 9: Surface resistance as function of RF magnetic field at 2.5 K and 400 MHz. The ECR coating is compared to a typical LHC coating and bulk Nb. Dashed lines indicate exponential (LHC) and linear (ECR film & bulk Nb) fits.

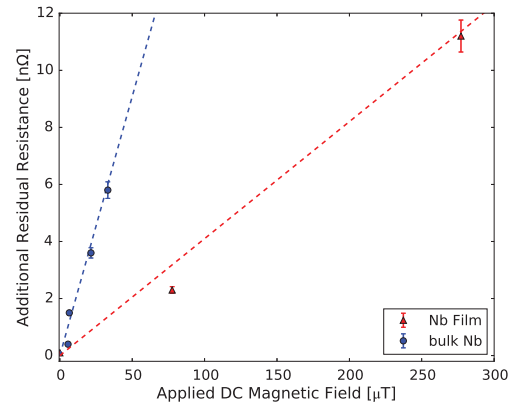


Figure 10: Additional residual resistance at 2.5 K and 400 MHz as function of ambient magnetic field. Dashed lines indicate linear fits through the origin.

Q-Slope

Besides the low field SRF properties, the surface resistance at 400 MHz was measured as a function of field at 4 K where the BCS part contributes significantly to R_S and at 2.5 K where the residual contribution dominates the overall losses. The field dependence is not only compared to the reactor grade bulk Nb but also to a typical magnetron sputtered LHC cavity which has also a resonance frequency of 400 MHz [22].

Figure 8 shows the surface resistance at 4 K. The LHC coating shows the typical exponential increase with RF field while the reactor grade bulk niobium sample shows a quadratic field dependence. We find that the increase of R_S with RF field for the ECR coating is comparable to the bulk niobium but still following an exponential trend. The offset between the ECR and LHC coating compared to the bulk niobium is due to the difference in residual resistance.

Figure 9 compares the surface resistance as function of RF field at low temperature. Even though the ECR coating performs comparably to bulk niobium at 4 K, the Q-slope is still stronger at 2.5 K. It is however flatter than the LHC coating and the surface resistance follows a linear trend rather than an exponential one.

Effect of Trapped Magnetic Flux

The Quadrupole Resonator is equipped with a small solenoid inside the thermometry chamber which allows applying a dc magnetic field to the sample surface. Figure 10 shows the additional low field residual resistance at 400 MHz of the ECR coating and the reactor grade bulk Nb sample due to trapped flux. It can be seen that the trapped flux sensitivity for the niobium film is still significantly lower (about a factor of 4.6) than for the bulk sample of similar RRR. This would be consistent with larger pinning centers, for instance thicker grain boundaries [23]. Specifically, the trapped flux sensitivity of the ECR film is consistent with a pinning centre size 3.5 larger than for RRR 300 bulk Nb. For comparison, trapped flux measurements on the 1.5 GHz magnetron sputtered Nb/Cu cavities are consistent with relative pinning centre sizes between 1.9 and 7.2 depending on the cavity [4].

Effect of Thermal Cycling on the Residual Resistance

The effect of thermal cycling on the surface resistance is extensively studied and discussed for bulk niobium [24–26]. In this context, two aspects have to be taken into account: the efficiency of the Meissner effect depending on the transition dynamics to the superconducting state and thermo-electric currents and corresponding dc magnetic field that might be induced due to a thermal gradient across the cavity during

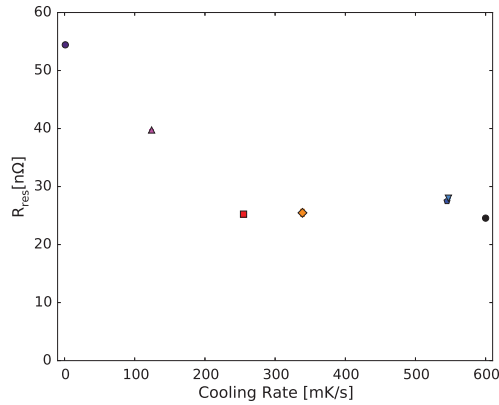


Figure 11: Low field surface resistance at 2.0 K and 400 MHz as function of cooling rate.

cool down. In both cases, the change in residual resistance is due to a change in trapped magnetic flux.

In the Quadrupole Resonator the sample can be (independently of the host cavity) warmed up to the normal conducting state and the cooling dynamics can be defined by changing the dc heating during cool down. The cooling speed and the (radial) temperature gradient across the sample can however not be changed independently. The cooling speed is defined at the moment when the temperature sensor crosses T_c . Since all temperature sensors have the same distance to the heater, the spacial gradient can only be simulated and is estimated to range from 7 mK/cm for very slow cool down to 33 mK/cm for the fastest cool down. Figure 11 shows the low field surface resistance at 400 MHz and 2.0 K as function of the cooling rate. It can be seen that for slow cooling resp. smaller spatial temperature gradient the surface resistance increases by more than 30 nΩ resp. a factor of 2 compared to fast cooling. The lowest R_S was even measured after quenching the sample which yielded the fastest cooldown rate. The same measurement was done on the reactor grade bulk Nb sample which showed a decrease in surface resistance of about 2 nΩ with slow cooling which is consistent with a more efficient Meissner effect [19].

The residual field in the QPR cryostat due to imperfect shielding is about 2 μT. It is clear from the coating's trapped flux measurement that the additional 30 nΩ for slow cooling cannot be just due to a change in the efficiency of the Meissner effect as it would require an ambient field in the order of 700 μT. We assume that the strong dependence of the residual resistance on the cooling dynamics is caused by magnetic fields induced by thermo-electric currents at the niobium-copper interface. A dedicated study is however needed to support this conclusion.

Effect of Thermal Cycling on the Q-Slope

Besides the influence of thermal cycling on the residual resistance, the effect on the Q-slope was also studied. Figure 12 displays the increase of surface resistance at 2.0 K and

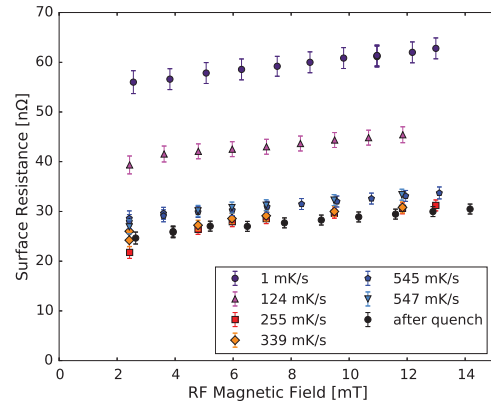


Figure 12: Linear Q-slope as a function of RF field for different thermal cycles.

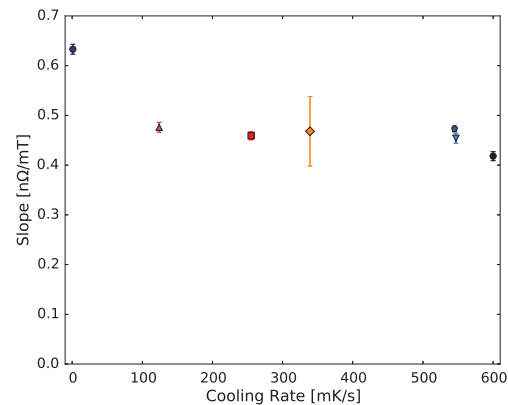


Figure 13: Linear Q-slope as function of cooling rate.

400 MHz for different cooling cycles. At such a low temperature and frequency, R_S follows a linear trend. All presented $R_S(B)$ curves were fitted linearly and the resulting Q-slope parameter is plotted as function of cooling rate in Figure 13. Not only does the overall surface resistance decrease for faster cooling but also the Q-slope flattens for the best cooling conditions. The latter is in qualitative agreement with recent results on the Nb/Cu cavities of the HIE-Isolde project [27].

CONCLUSION

The Nb/Cu technology has recently been making progress in growing denser films. We report on a Nb coating with bulk-like characteristics that performs at 4 K and 400 MHz comparable with bulk Nb. However, the Nb film typical Q-slope is still present at 2.5 K even though mitigated. Moreover, it is found that this Nb film is still less sensitive to trapped flux than comparable bulk Nb. In contrast to that, the effect of thermal cycling on the surface resistance is by far stronger than for bulk Nb. We also find that the thermal cycling not only acts on the low field resistance but also on the steepness of the Q-slope. The results cannot be explained

by the efficiency of the Meissner effect. We assume therefore that thermo-electric currents at the Nb-Cu interface create large magnetic field which are trapped in the film.

From comparing the microstructure of Nb films with their SRF performance, we identify a low crystal defect density and an excellent adhesion as key aspects in the quest for Q-slope free Nb/Cu cavities.

ACKNOWLEDGMENT

We thank B. Bartova and the team of EPFL-CIME for the FIB-SEM images of the HIE-Isolde coatings, R. Valizadeh for the FIB-SEM images of the ECR coating and R. Crooks from Black-Labs LLC, for the EBSD measurements on the ECR Nb/Cu film. We thank J. Bremer, L. Dufay-Chanant and T. Köttig for providing the cryogenic infrastructure and technical help, as well as G. Pechaud, S. Forel and T. Tardy for preparing the samples for the tests in the QPR. This work is sponsored by the Wolfgang Gentner Programme of the German Federal Ministry of Education and Research (BMBF).

REFERENCES

- [1] C. Benvenuti, N. Circelli, and M. Hauer. Niobium Films for Superconducting Accelerating Cavities. *Applied Physics Letters*, 45(5):583–584, 1984.
- [2] J. Halbritter. On Surface Resistance of Superconductors. *Zeitschrift fuer Physik*, 266(3):209–217, 1974.
- [3] O. Bruening, J. Poole, P. Collier, P. Lebrun, R. Ostojic, S Myers, and P. Proudlock. The LHC Main Ring. *LHC Design Report*, 1, 2004.
- [4] C. Benvenuti, S. Calatroni, I. E. Campisi, P. Darriulat, M. A. Peck, R. Russo, and A.-M. Valente. Study of the Surface Resistance of Superconducting Niobium Films at 1.5 GHz. *Physica C*, 316(3):153–188, 1999.
- [5] M. Pasini, S. Calatroni, N. Delruelle, M. Lindroos, V. Parma, and P. Trilhe. MOP028. In *Proceedings of the LINAC'08*, pages 124–126, Victoria, Canada, 2008.
- [6] Y. P. Purandare, A. P. Eghasarian, and P. Eh. Hovsepian. Deposition of nanoscale multilayer CrN/NbN physical vapor deposition coatings by high power impulse magnetron sputtering. *Journal of Vacuum Science & Technology A: Vacuum, Surfaces, and Films*, 26(2):288, 2008.
- [7] M. Krishnan, E. Valderrama, B. Bures, K. Wilson-Elliott, X. Zhao, L. Phillips, A.-M. Valente-Feliciano, J. Spradlin, C. Reece, and K. Seo. Very high residual resistivity ratios of heteroepitaxial superconducting niobium films on MgO substrates. *Superconductor Science and Technology*, 24(11):115002, November 2011.
- [8] I.G. Brown. Vacuum arc ion sources. *Review of Scientific Instruments*, 65(10):3061, 1994.
- [9] G. Wu, A.-M. Valente, H.L. Phillips, H. Wang, A.T. Wu, T.J. Renk, and P. Provencio. Studies of niobium thin film produced by energetic vacuum deposition. *Thin Solid Films*, 489(1-2):56–62, October 2005.
- [10] G. Terenziani, S. Calatroni, T. Junginger, I. A. Santillana, and A. P. Eghasarian. TUP078. In *Proceedings of the SRF'13*, Paris, France, 2013.
- [11] A. Sublet, B. Bartova, S. Calatroni, T. Richard, G.J. Rosaz, and M. Taborelli. TUPB027. In *Proceedings of SRF'15*, Whistler, Canada, 2015.
- [12] A. Sublet, I. Aviles, S. Calatroni, P. Costa Pinto, N. Jecklin, S. Prunet, A. Sapountzis, W. Venturini Delsolaro, and W. Voltenberg. TUP077. In *Proceedings of SRF'13*, pages 617–620, Paris, France, 2013.
- [13] B. Bartova, S. Calatroni, A. Sublet, M. Taborelli, A.B. Aebbersold, D.T.L. Alexander, and M. Cantoni. WEPHA022. In *Proceedings of the IPAC'15*, pages 3155–3158, 2015.
- [14] A. Anders. A structure zone diagram including plasma-based deposition and ion etching. *Thin Solid Films*, 518(15):4087–4090, May 2010.
- [15] G. Wu, H.L. Phillips, and R.M. Sundelin. Energetic deposition of niobium thin film by ecr-plasma. *Journal of Vacuum Science & Technology A: Vacuum, Surfaces, and Films*, 21(4):842, 2003.
- [16] A.-M. Valent-Feliciano. PhD thesis. Université Paris XI, 2014.
- [17] E. Mahner, S. Calatroni, E. Chiaveri, E. Haebel, and J. M. Tessier. A new instrument to measure the surface resistance of superconducting samples at 400 MHz. *Rev Sci Instrum*, 74(7):3390, 2003.
- [18] T. Junginger, W. Weingarten, and C. Welsch. Extension of the Measurement Capabilities of the Quadrupole Resonator. *Rev Sci Instrum*, 83, 2012.
- [19] S. Aull, S. Doebert, T. Junginger, and J. Knobloch. WEIOC01. In *Proceedings of SRF'13*, pages 779–782, Paris, France, 2013.
- [20] A.T. Perez Fontenla. EDMS1462196. Tech. Report EDMS 1462196, CERN, Geneva, Switzerland, January 2015.
- [21] A. B. Pippard. An Experimental and Theoretical Study of the Relation between Magnetic Field and Current in a Superconductor. *Proceedings of the Royal Society A: Mathematical, Physical and Engineering Sciences*, 216(1127):547–568, February 1953.
- [22] S. Bauer, W. Diete, B. Griep, M. Peiniger, H. Vogel, P. vom Stein, S. Calatroni, E. Chiaveri, and R. Losito. WEP016. In *Proceedings of the SRF'99*, pages 437–439, Santa Fe, USA, 1999.
- [23] S. Aull and J. Knobloch. Depinning of Trapped Magnetic Flux in Bulk Niobium SRF Cavities. <http://arxiv.org/abs/1507.04105>, 2015.
- [24] O. Kugeler, A. Neumann, S. Voronenko, W. Anders, J. Knobloch, M. Schuster, A. Frahm, S. Klauke, D. Pflueckhahn, and S. Rotterdam. TUPPO053. In *Proceedings of the SRF'09*, pages 352–354, Berlin, Germany, 2009.
- [25] J.-M. Vogt, O. Kugeler, and J. Knobloch. High Q Operation of Superconducting RF Cavities: Potential Impact of Thermocurrents on the RF Surface Resistance. *Physical Review Special Topics - Accelerators and Beams*, 18(4), April 2015.
- [26] M. Martinello, A. Romanenko, M. Checchin, A. Grassellino, A. C. Crawford, A. Melnychuk, and D. A. Sergatskov. arXiv:1504.04441. 2015.
- [27] P. Zhang, Y. Kadi, A. Miyazaki, M. Therasse, and W. Venturini Delsolaro. TUPB077. In *Proceedings of the SRF'15*, Whistler, Canada, 2015.